J Pathol Inform

Editor-in-Chief:
Anil V. Parwani , Pittsburgh, PA, USA
Liron Pantanowitz, Pittsburgh, PA, USA

OPEN ACCESS
HTML format

For entire Editorial Board visit : www.jpathinformatics.org/editorialboard.asp

Original Article

Computer-assisted imaging algorithms facilitate histomorphometric quantification of kidney damage in rodent renal failure models

Marcin Klapczynski, Gerard D. Gagne, Sherry J. Morgan[1], Kelly J. Larson[2], Bruce E. LeRoy, Eric A. Blomme, Bryan F. Cox[2], Eugene W. Shek[2]

Investigative Toxicology and Pathology, [1]Preclinical Safety, [2]Integrative Pharmacology, Abbott Laboratories, 100 Abbott Park Rd, Abbott Park, IL 60064, USA

E-mail: *Marcin Klapczynski - marcin.klapczynski@abbott.com
*Corresponding author

Received: 27 January 12 Accepted: 04 April 12 Published: 28 April 12

This article may be cited as:
Klapczynski M, Gagne GD, Morgan SJ, Larson KJ, LeRoy BE, Blomme EA, *et al.* Computer-assisted imaging algorithms facilitate histomorphometric quantification of kidney damage in rodent renal failure models. J Pathol Inform 2012;3:20.

Available FREE in open access from: http://www.jpathinformatics.org/text.asp?2012/3/1/20/95456

Copyright: © 2012 Klapczynski M. This is an open-access article distributed under the terms of the Creative Commons Attribution License, which permits unrestricted use, distribution, and reproduction in any medium, provided the original author and source are credited.

Abstract

Introduction: Surgical 5/6 nephrectomy and adenine-induced kidney failure in rats are frequently used models of progressive renal failure. In both models, rats develop significant morphological changes in the kidneys and quantification of these changes can be used to measure the efficacy of prophylactic or therapeutic approaches. In this study, the Aperio Genie Pattern Recognition technology, along with the Positive Pixel Count, Nuclear and Rare Event algorithms were used to quantify histological changes in both rat renal failure models. **Methods:** Analysis was performed on digitized slides of whole kidney sagittal sections stained with either hematoxylin and eosin or immunohistochemistry with an anti-nestin antibody to identify glomeruli, regenerating tubular epithelium, and tubulointerstitial myofibroblasts. An anti-polymorphonuclear neutrophil (PMN) antibody was also used to investigate neutrophil tissue infiltration. **Results:** Image analysis allowed for rapid and accurate quantification of relevant histopathologic changes such as increased cellularity and expansion of glomeruli, renal tubular dilatation, and degeneration, tissue inflammation, and mineral aggregation. The algorithms provided reliable and consistent results in both control and experimental groups and presented a quantifiable degree of damage associated with each model. **Conclusion:** These algorithms represent useful tools for the uniform and reproducible characterization of common histomorphologic features of renal injury in rats.

Key words: 5/6 nephrectomy, adenine kidney model, digital pathology, digital slide, Genie, image analysis, rodent renal failure model

Access this article online

Website: www.jpathinformatics.org

DOI: 10.4103/2153-3539.95456

Quick Response Code:

INTRODUCTION

Context and Aims

Advanced computer image analysis capabilities can be employed for automated measurement of pathological microscopic changes in kidneys affected by a disease process.

The purpose of this study was to evaluate a set of image analysis tools for histopathological analysis of kidney damage and to examine the process of effective practical implementation.

Whole slide imaging (WSI) is based on analysis of glass slides scanned by a high-resolution digital camera. The digital slides are stored on a dedicated server which facilitates availability for on-line telepathology or image analysis. WSI is steadily gaining popularity in daily practice of pathology; however, the adoption of digital pathology has lagged in comparison to the comparable transition to digital radiology due to several logistical and technical hurdles.[1] A key advantage of digital slides over glass slides is their facilitation of the use of computer-aided diagnostic image algorithms,[2] which can be automated and provide consistency and accuracy often greater than light microscopy,[3,4] while showing excellent correlation with manual interpretations.[5]

Kidney disease is one of the most common causes of illness in humans.[6] The kidney is susceptible to a wide variety of pathologic acute and chronic processes. Acute kidney injury is common in patients admitted to intensive care units and is the result of various injuries, such as severe blood loss, circulatory collapse, and infectious processes. Chronic renal diseases are important sequelae of widespread comorbidities, such as diabetes mellitus, and hypertension.[6,7] To further understanding of the underlying mechanisms of renal disease and to evaluate the efficacy of novel therapeutic agents, animal models of renal disease are commonly used in both academic and pharmaceutical research environments. Two commonly used models are the 5/6 nephrectomy and adenine-induced renal failure.

In recent years, automated image analysis has been employed for renal prophylactic and therapeutic approaches. Automated quantification of microvascular density has been utilized as an independent measure of renal cell carcinoma aggressiveness, overcoming previous limitations of manual evaluation within a small area of a tumor.[8] Digital evaluation of complement C4d component deposition in kidney allograft core needle biopsies showed improved reproducibility of the scoring, comparing to the manual pathologist's evaluation.[9] Quantification of interstitial fibrosis by image analysis in renal transplantation has been demonstrated as a reliable and reproducible method in routine practice, assisting in early diagnosis of the interstitial lesions of chronic allograft injury, as well as a predictive tool of long-term transplant function.[10,11] In this study we developed and evaluated image analysis tools to quantify histopathological changes in the kidneys of rat models of renal failure.

The Rat 5/6 Nephrectomy Model[12]

It is one of the most commonly used animal models of progressive renal failure. The reduction of renal mass (and therefore nephron number) is accomplished by surgical excision of both poles of one kidney, and removal of the contralateral kidney. Nephrons in the remnant kidney undergo compensatory functional and structural adaptive changes. Renal injury is caused by glomerular hypertension resulting from increased glomerular capillary hydraulic pressure secondary to the accumulation of extracellular matrix.[13]

Subtotal nephrectomy reduces creatinine clearance by 60% and increases serum parathyroid hormone (PTH) and phosphate concentrations 12-fold and 2.7-fold respectively.[14] High-phosphate intake worsens the secondary hyperparathyroidism and vasodilatation (as evidenced by the morphology of small mesenteric arteries). A high-phosphate (1.5%) diet causes further elevation of serum PTH and phosphate concentrations (33-fold and 5.5-fold, respectively)[14] and is associated with hyperplasia of the parathyroid glands.[15] Nephrectomized animals also present with arterial hypertension, which when coupled with phosphorus overload can result in myocardial hypertrophy.[16]

Rat Model of Adenine-Induced Kidney Failure

Chronic dietary administration of adenine in rats (0.75% diet for four weeks) results in azotemia, accumulation of uremic toxins, dysregulation of amino acids and electrolyte homeostasis, and PTH imbalances.[17] The histopathological findings in the kidneys of adenine-fed rats indicate injury to proximal tubules, some distal tubules and glomeruli.[17] Adenine-fed rats also develop ectopic calcification and altered serum concentrations of relevant renal analytes including phosphate, creatinine, PTH, and blood urea nitrogen (BUN).[18]

METHODS

5/6 Nephrectomy (5/6 NX) procedures, involving surgical removal of one kidney and 2/3 of the other kidney, were performed by Charles River Laboratories (Portage, MI, USA). Control animals underwent a sham procedure consisting of general anesthesia and abdominal incision with gentle manipulation of viscera. After 6 weeks of acclimation, the rats (five per group) were randomized to receive either a regular (0.6% phosphate, 0.6% calcium) or high-phosphate (1.2% phosphate, 0.6% calcium) diet for 6 to 8 weeks.

The Adenine-Induced Kidney Failure (AIKF) model was analyzed in two separate studies. Male Sprague-Dawley rats were provided by Charles River Laboratories. A 5-day study (AIKF 5D) involved three groups (four rats per group): control (administered vehicle only; 0.5% methylcellulose), low dose (200 mg/kg/day) and high dose (300 mg/kg/day) of adenine sulfate (Sigma-Aldrich, St. Louis, MO, USA).

A 10-day study (AIKF 10D) included two groups: control (administered vehicle only; 0.5% methylcellulose) and a group orally gavaged a 100 mg/day dose (which corresponds to 200 mg/kg/day for a 500 g rat). Five

animals from the control group and four animals from the treated groups (due to premature deaths) were analyzed.

After completion of the above studies, animals were euthanized and multiple tissues types collected for histopathology. Blood was collected for serum chemistry analysis (BUN, creatinine, Ca^{2+}, PO_4^{2-}). Experiments were conducted in accordance with guiding principles in the use of animals in toxicology (2002) and were approved by the local Institutional Animal Care and Use Committee.

Tissue Processing

Tissues collected for histological analysis were fixed in 10% neutral buffered formalin overnight and then paraffin embedded in a tissue processor. Formalin-fixed paraffin-embedded kidneys were sectioned at 4 μm and mounted on Superfrost Plus slides (Thermo, Portsmouth, NH, USA). Sections were stained with hematoxylin and eosin (H&E) or used for immunohistochemistry (IHC) using either a Mouse-anti-Rat-Nestin antibody (Millipore, Billerica, MA, USA) or a Rabbit-anti-PMN antibody (Accurate Chemical and Scientific Corp, Westbury, NY, USA). Sections were subject to antigen retrieval in 0.1 M citrate buffer in a steamer for 20 minutes, followed by slow cool-down for another 20 minutes. To obtain uniform and consistent IHC staining, slides were then processed in IntelliPath Automated Slide Stainer (Biocare Medical, Concord, CA, USA). Sections were incubated in the following solutions, and washed once with TBS-Tween 20 (0.1%) between the steps: 3% hydrogen peroxide solution for 10 minutes; Avidin (Vector Labs, Burlingame, CA, USA) for 15 minutes, Biotin (Vector Labs) for 15 minutes, then blocked in 10% secondary antibody host serum (Vector Labs) in TBS with 3% BSA for 30 minutes. Primary antibodies were diluted in Antibody Diluent (Dako, Carpinteria, CA, USA) at 1:200 (mouse-anti-rat-nestin) or 1:400 (rabbit-anti-PMN antibody) and sections were incubated in the solution for up to 60 minutes, followed by three washes in TBS-Tween 20 (0.1%). Sections were then incubated in an appropriate secondary antibody solution, biotin conjugated (Vector Labs) for 30 minutes, washed as above, then incubated in streptavidin-HRP solution from the Vectastain ABC kit (Vector Labs), and washed as above. Chromogen (3,3' diaminobenzidine DAB) reaction was performed using intellipath FLX™ DAB Chromogen Kit (Biocare Medical) for 5 minutes. Sections were then washed in deionized water and counterstained with hematoxylin 7211 for 3 minutes, dehydrated, and coverslipped.

Slides Digitization and Analysis

Digital images from the experimental glass slides were obtained using ScanScope Digital Slide Scanner (Aperio, Vista, CA, USA) at a 20× magnification (mag) and archived on the devoted Spectrum Server V10.2.2.2315 (Aperio). Quality control of the scanned images and all further analysis were performed using ImageScope V10.2.1.2315 (Aperio). Slides were analyzed by using one of the following algorithms: Genie v1_v10.0.0.1798, Positive Pixel Count v9_v10.0.0.1805, Nuclear v9_v10.0.0.1798, or Rare Event Detection v1_v10.0.0.1798. Genie (GENetic Imagery Exploration) is a pattern recognition algorithm that learns to distinguish morphological features based on objects (called classes) provided by the user in a training set. After testing the classifier, the classes can then be selected for subsequent analysis using specific task algorithms. The Positive Pixel Count algorithm counts pixels of predetermined color, intensity and saturation. The Nuclear algorithm is optimized to identify cell nuclei of declared size, color, roundness or compactness. The Rare Event Detection algorithm is optimized to localize distinct objects of predetermined features mentioned in the previous algorithms. A brief description and range of parameters used in the algorithms is provided in Table 1. The remaining parameters not specified in each of the following algorithms were set at the default values.

Histopathological Changes [Figure 1]

The following histological endpoints were assessed in

Table 1: Parameters used in the image analysis algorithms (adapted from Aperio documentation)

Parameter	Description	Value Range
Roundness	The ratio of the area of a nucleus to the area of a circle that fully encloses that nucleus	0 – 1 (perfect circle)
Compactness	The ratio of area of a nucleus to the area of a circle with a circumference equal to the perimeter of that nucleus	0 – 1 (perfect circle)
Elongation	The ratio of the min/max principal moments of the nuclei (a quantitative measure of the shape of a set of points)	0 – 1 (perfect circle)
Nuclear size	Min/Max determines the nuclei size limits in um^2	0 – user defined
Object pixels	Min/Max determines the object size limits in pixels	0 – user defined
Hue value	The color of the objects of interest. It is a number of a desired color indicated in radial value on an arbitrary color wheel, divided by 360	0 – 1
Hue width	Range of hues, centered on the Hue Value that will satisfy the hue detection process	0 – 360
Color saturation	The amount of color defined by the Hue Value. RGB values are represented as gray + color	0 – 1 (fully saturated, no gray component)
Intensity	The measure of brightness of a pixel	0 – 255 (bright white)

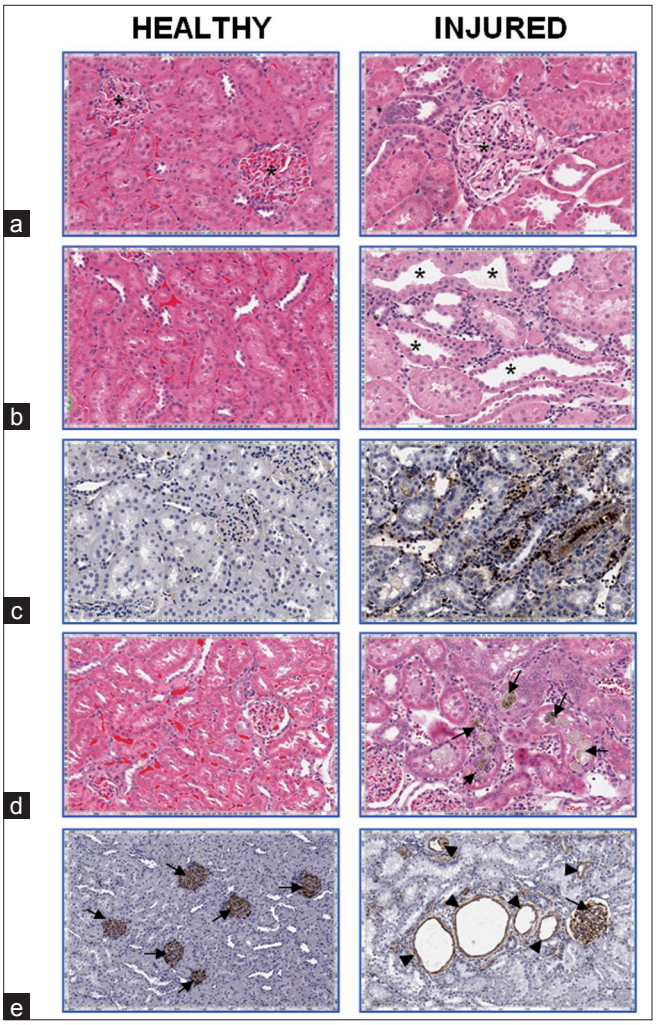

Figure 1: Histopathologic findings selected for image analysis in the 5/6 nephrectomy and adenine models: (a) expansion of glomeruli (asterisks), (b) tubular dilation (asterisks), degeneration and regeneration, (c) interstitial inflammation/fibrosis, (d) mineral aggregation (arrows), and (e) specific biomarker expression changes – glomerular (arrows) and non-glomerular (arrowheads) nestin immunostaining. The pictures in rows a, b, c, d are displayed at 20x mag, the pictures in row E are at 14× mag

both renal failure models and subjected to image analysis: (1) Glomerular expansion, which was characterized as an increased amount of eosinophilic-staining material in glomeruli. These changes may represent cytoplasmic hypertrophy of mesangial cells or excessive extracellular matrix production and deposition. (2) Tubular dilatation, degeneration, and regeneration resulting from injury to tubular epithelial cells leading to cell death and stimulation of regenerative processes. Commonly there is evidence of regrowth of epithelium which morphologically appears flattened and gives the tubules a dilated appearance. (3) Interstitial inflammation/fibrosis: tubular injury leads to inflammation evidenced by the infiltration of neutrophils, macrophages, and lymphocytes. Proliferation of fibrous connective tissue occurs with chronicity. (4) Mineral aggregation: in the adenine model, this represents precipitation of the compound (2,8-dihydroxyadenine). (5) Specific biomarker changes: nestin immunohistochemistry (IHC) is useful to identify injury to a particular cell type. In the mature, healthy kidney, podocytes are the only cells expressing nestin. In injured kidneys, nestin expression is also observed in renal tubular cells and tubulointerstitial myofibroblasts during the progression to tubulointerstitial fibrosis.[19]

Glomerular Cell Density [Figure 2-1] and NonGlomerular Nestin Staining [Figure 2-2]

To enhance reliable glomerular identification by Genie, IHC was performed using an anti-nestin antibody. Classes included in the Genie training set were glomeruli (glomeruli, including Bowman space), other kidney tissue (tubules, blood vessels, and interstitial tissue), other labeled kidney tissue (DAB-stained tubules and interstitial tissue), red blood cells (RBC), slide glass. Separate classifier sets were developed for each healthy and injured tissue, due to significant DAB staining in interstitial regions of the latter resulting in a lack of reproducibility of the genie learning algorithm. The classifier was then used for subsequent analysis. The glomeruli class was analyzed by Nuclear algorithm, with the following settings: min nuclear size = 5 μm^2, max nuclear size = 4.e+006 μm^2, min roundness = 0.1, min compactness = 0, min elongation = 0.1. The wide range of predefined nuclear size facilitated detection of several cell types, which vary by size and distribution. The lower limit allowed for the detection of most glomerular granular and mesangial cells, whereas the upper limit enabled to localize podocytes along with pedicels. This provided a collective score reflecting total glomeruli cellularity. Low roundness threshold enhanced detection of flat epithelium and podocyte cells. All of the detected nuclei were counted and normalized by the Glomeruli class area (total glomeruli area detected by Genie, represented in pixels), and averaged for the treatment group.

For the nonglomerular nestin staining, the Glomeruli class was excluded from the analysis. The remaining kidney tissue was analyzed by Positive Pixel Count algorithm, with the hue value = 0.1 and hue width = 0.5, color saturation = 4.e-002, counting all positive DAB-stained pixels, including all intensities. Pixel number was then normalized by the whole kidney section area (um^2) and averaged for the treatment group.

Tubular Lumen Measurement [Figure 2-3]

The analyzed slides were H&E stained. The Genie training set criteria included: collecting tubules (visible white lumen), convoluted tubules (no distinct white lumen), glomeruli, RBC, and slide glass. The collecting tubules and slide glass classes were analyzed by Positive Pixel Count algorithm, with the hue value = 0.7 and hue width = 0.5, color saturation = 4.e-002, counting all negative

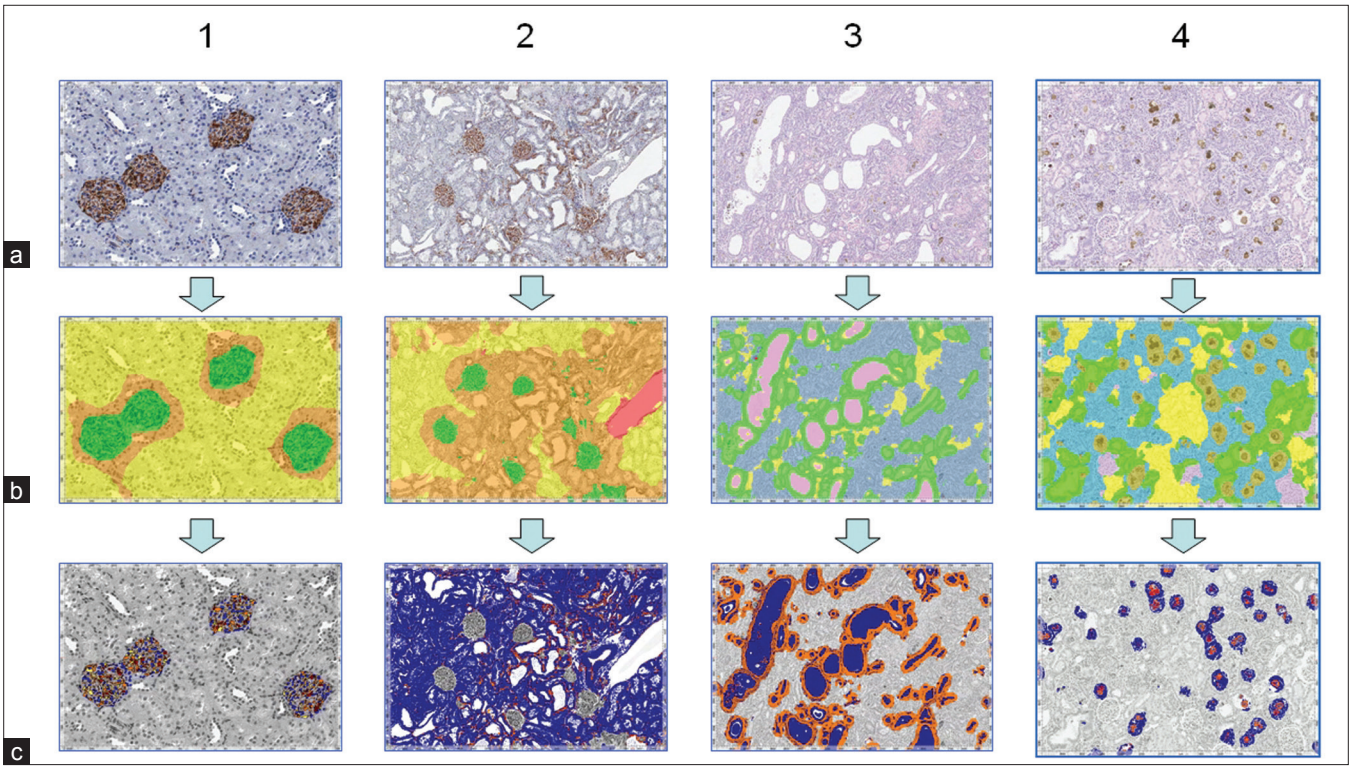

Figure 2: Image analysis using Genie pattern recognition technology. (1) Nestin IHC stained podocytes (a), allowed Genie to recognize glomeruli more specifically (b). The Glomeruli detection algorithm was then used as a classifier for subsequent analysis. The Nuclear algorithm was used to count nuclei in the classified regions (c). (2) Genie was used to identify glomeruli (a, b), which were then excluded from subsequent analysis. Non-glomerular nestin expression (DAB) was quantified by the Positive Pixel Count algorithm in the non-glomerular classifier (c). (3) Genie was trained to recognize dilated tubules on H&E stained kidney sections (a, b) and used them as a classifier for Positive Pixel Count algorithm. White pixels (tubular lumen) were counted (c). (4) Genie was trained to recognize mineral aggregates on H&E stained kidney sections (a, b) and used them as a classifier for Positive Pixel Count algorithm. Brown pixels (crystals) were counted (c). The pictures are displayed at following magnification: 1: 20×; 2 and 3: 6.5×; 4: 10×

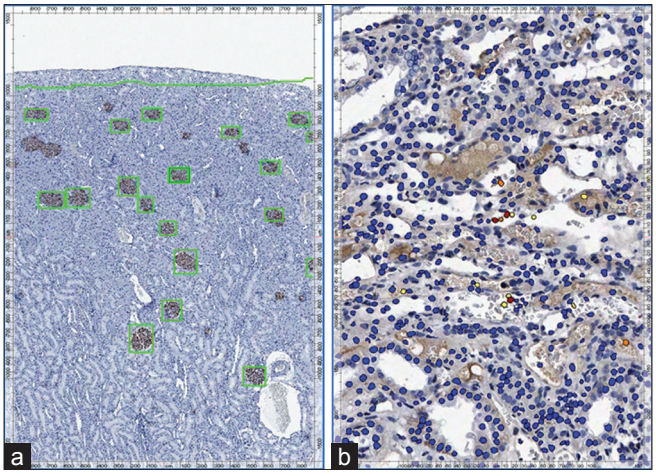

Fiugre 3: Image analysis using Aperio tools without Genie. Rare Event Detection algorithm was used to detect, count and report area of nestin-stained glomeruli (a). IHC with a polyclonal anti-PMN antibody was used to identify neutrophil granulocytes. Nuclear algorithm was used to count immunostained neutrophils (positive nuclei are highlighted in orange and brown) (b). Picture A is displayed at 4× mag, B is at 20× mag

(white) lumen pixels. Only the cortico-medullary region was analyzed, while the renal papilla was excluded from analysis due to significant inter-sample variability. Inclusion of renal papilla would introduce inconsistent false positive data into the analysis results. The size of renal papilla varies significantly across specimens, as a consequence of deviation in the tissue dissection, trimming, embedding and sectioning. Including renal papilla would bring in an undesirable variation in area of analysis to which the data are normalized. In addition, papillary tubules would be falsely identified as dilated, which does not indicate tissue injury in this location. The pixel number was then normalized by the analysis area (total number of pixels) and averaged for the treatment group.

Mineral Aggregate Accumulation [Figure 2-4]

The analyzed slides were H&E stained. The Genie training set criteria included mineral deposits, collecting tubules, convoluted tubules, glomeruli, granular interstitial cells, RBC, and slide glass. The mineral deposits class was analyzed by positive pixel count algorithm, with the hue value = 0.1, hue width = 0.5, and color saturation = 4.e-002, counting all positive (brown) crystal pixels. Pixel number was then normalized by the cortical kidney section area (total number of pixels) and averaged for the treatment group. The renal papilla was excluded from the analysis due to significant intersample variability, as explained above.

Glomerular Expansion [Figure 3a]

Rare Event detection algorithm was used to detect, count and report area of nestin-immunolabeled glomeruli. The algorithm is very sensitive to minor changes in tissue staining intensity. Thus, each digital slide was pre-tested on a small representative area, then after adjusting the critical parameters, the whole slide image analysis was performed. The ranges of the parameters were: hue value: 0.1, hue width: 0.38 – 0.54, color saturation: 0.02 – 0.07, roundness: 0.35 – 0.41, intensity: 209 - 217. Lower and upper limits were set for the object size to avoid false positives, such as stained interstitial tissue or clustered glomeruli. Min object pixels was set at 15000 and max object pixels at 80000. For the statistical analysis, the reported area was averaged for each animal, then for the treatment group.

PMN Infiltration [Figure 3b]

Nuclear algorithm was used to identify immunohistochemically stained neutrophils as positive nuclei, with min roundness = 0.65, min compactness ranging from 0.4 to 0.6, and using IHCNuclear Classifier. Positive nuclei of strong and moderate staining were counted, normalized by total section area (total number of pixels) and averaged for the treatment group.

Statistical Method Used

Student's *t*-test was used to evaluate statistical significance of changes comparing to control (CI=95) using custom Excel worksheet. Sample correlation coefficient was used to estimate correlation between pathologist's evaluation and automated image analysis.

RESULTS

Serum Chemistry [Table 2]

In the 5/6 nephrectomy model, BUN, creatinine, and phosphorus serum levels were increased by 3.4, 1.9, 1.2-fold respectively in the low phosphate diet. In the high phosphate diet there was correspondingly, 6.8, 3.6, and 1.8-fold increase in those values. In the adenine model there was elevation of BUN (2.4 for 200 mg/kg/day and 2.6 for 300 mg/kg/day) and creatinine (1.7 for 200 mg/kg/day and 2.0 in 300 mg/kg/day) in the 5-day model. The increase of BUN, creatinine, and phosphorus was more pronounced in the 10-day model (8.7, 6.5, and 1.9-fold change respectively).

Histological Findings Using Computer Image Analysis

In the 5/6 nephrectomy model, glomerular cellularity was slightly decreased reflecting glomeruli matrix accumulation as well as cell loss due to progressive renal failure changes [Figure 4a]. Nestin staining intensity was closely correlated with the extent of tubular and interstitial damage, which was increased in all

Table 2: Serum chemistry results

Animal group	Urea mg/dL	Creatinine mg/dL	Ca mg/dL	Phos mg/dL	Value
SHAM P0.6	12.6	0.6	11.3	6.8	mean
	0.9	0.0	0.2	0.3	SEM
5/6 NX P0.6	42.6	1.0	11.7	8.3	mean
	1.8	0.0	0.1	0.3	SEM
	3.4	1.9	1.0	1.2	fold change[a]
SHAM P1.2	11.0	0.5	11.3	5.7	mean
	0.6	0.0	0.2	0.4	SEM
5/6 NX P1.2	74.3	1.8	9.8	10.3	mean
	16.3	0.3	0.4	1.8	SEM
	6.8	3.6	0.9	1.8	fold change[a]
AIKF 5D VEHICLE	18.5	0.5	10.4	8.1	mean
	1.1	0.0	0.1	0.2	SEM
AIKF 5D 200 mg/kg/day	45.0	0.9	10.2	8.9	mean
	1.7	0.0	0.1	0.2	SEM
	2.4	1.7	1.0	1.1	fold change[b]
AIKF 5D 300 mg/kg/day	47.3	1.0	10.3	8.6	mean
	2.4	0.1	0.1	0.1	SEM
	2.6	2.0	1.0	1.1	fold change[b]
AIKF 10D VEHICLE	15.9	0.5	10.7	6.8	mean
	0.9	0.0	0.1	0.2	SEM
AIKF 10D 200 mg/day	137.9	3.3	11.2	13.1	mean
	12.0	0.3	0.2	0.9	SEM
	8.7	6.5	1.0	1.9	fold change[b]

[a]Fold change over SHAM control; [b]Fold change over vehicle

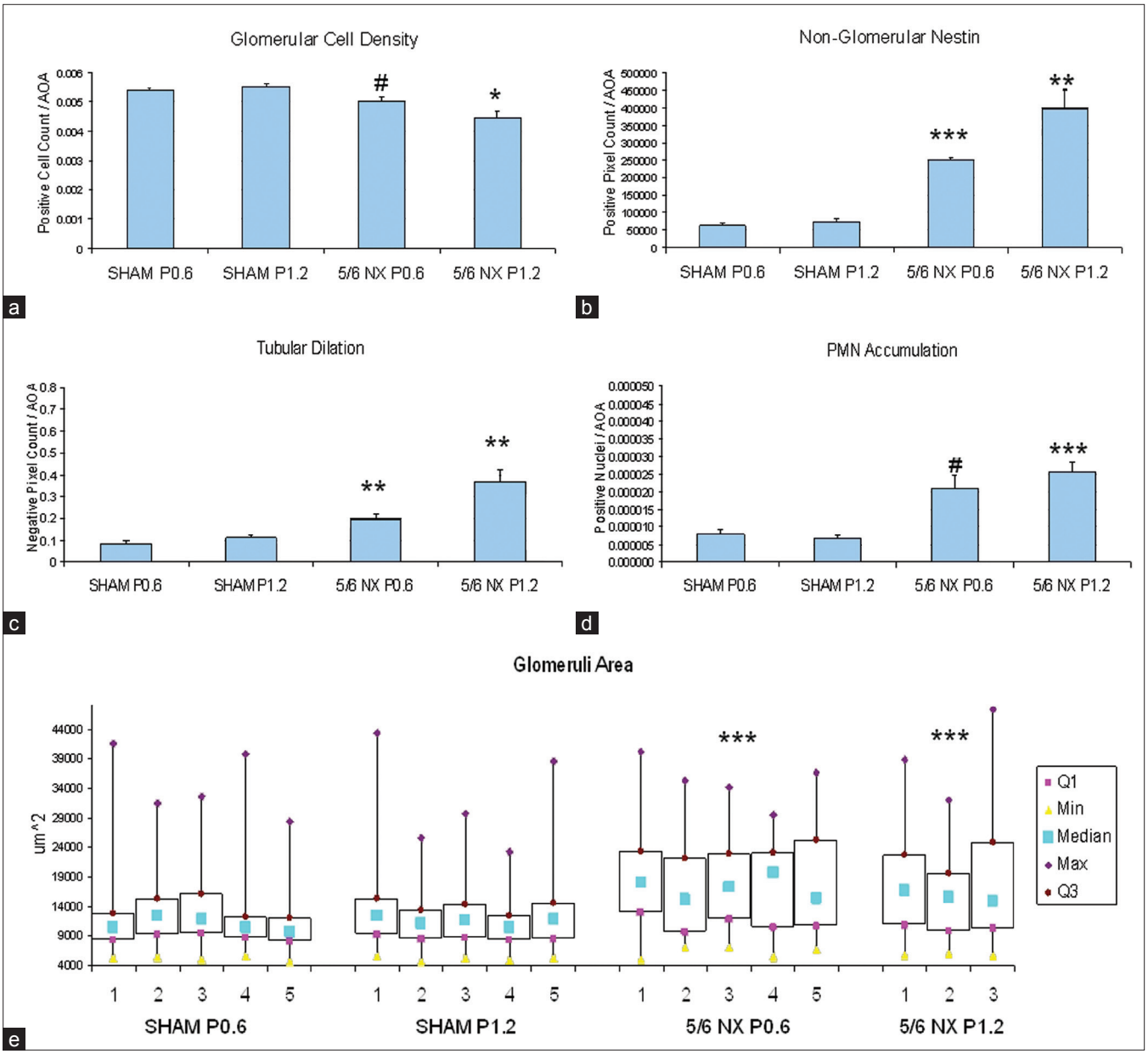

Figure 4: (a-e) Image analysis results for the 5/6 nephrectomy rat model. Error bars are SEM. *P*-values: #*P*<0.05, **P*<0.01, ***P*<0.005, ****P*<0.001, compared to the control (Student's *t*-test). For both of the sham and the 5/6 NX P0.6 groups *n*=5, *n*=3 for the 5/6 NX P1.2 group

experimental groups [Figure 4b]. Overall, kidney damage was more pronounced in the 5/6 nephrectomy model that received the high phosphate diet. The model exhibited tubular dilation [Figure 4c] which was more severe in rats fed a high phosphate diet. Tissue inflammation was only moderate [Figure 4d]. The nephrectomized rats showed a substantial increase in glomerular size [Figure 4e], which may reflect a model-specific glomerular hypertension. The increase in size was not further affected by the high phosphate diet.

In the adenine model, glomerular cellularity was also decreased [Figure 5a]. Nestin staining intensity revealed severe tubular and interstitial damage [Figure 5b]. Kidney damage was more pronounced in the AIKF 10D model, in which the pathological changes had more time to develop. Tubular dilation was more severe in those rats receiving prolonged administration of adenine [Figure 5c]. There was a time and dose-dependent accumulation of the crystalline adenine metabolite (2,8-dihydroxyadenine) [Figure 5e]. Inflammation was prominent, possibly due to the accumulated crystals stimulating a foreign body type reaction [Figure 5d]. Glomerular size was also slightly increased in the AIKF 5D study [Figure 5f].

Correlation Between Manual Evaluation and Automated Image Analysis [Table 3]

The H&E sections for all studies were analyzed by two pathologists, who evaluated appropriate histopathological

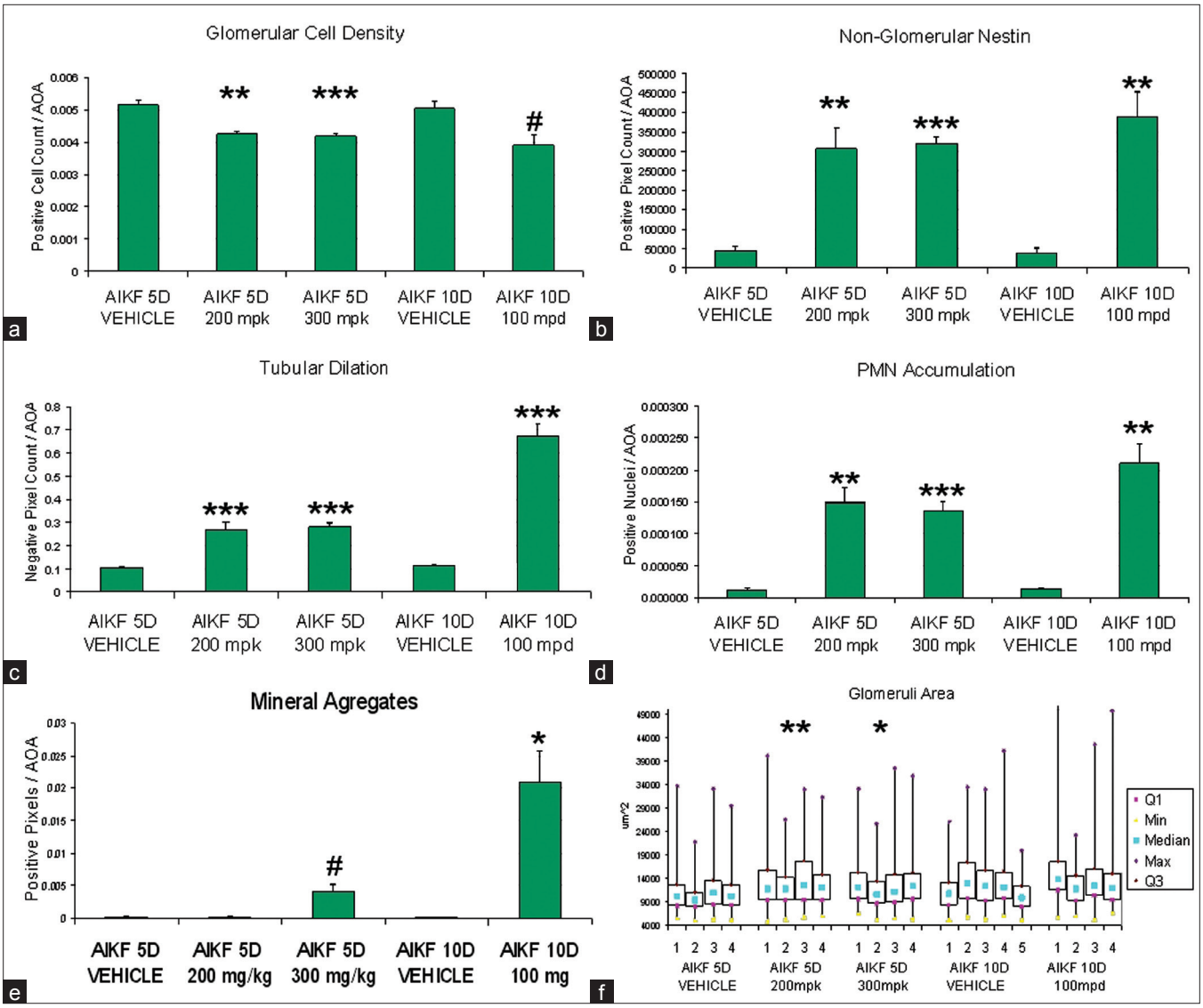

Figure 5: (a-f) Image analysis results for the adenine model. Mpk = mg/kg/day, mpd = mg/day. Error bars are SEM. *P*-values: #*P*<0.05, **P*<0.01, ***P*<0.005, ****P*<0.001, compared to the control (Student's *t*-test). *n*=4 for all groups, except for the vehicle group from 10-day study, where *n*=5

Table 3: Correlation coefficient of manual evaluation and automated image analysis. No glomerular changes were indicated in the AIKF models by the pathologist. No mineral aggregation analysis was performed on the 5/6 Nephrectomy model

	5/6 Nephrectomy	AIKF 5D	AIKF 10D
Glomerular Expansion	0.87	N/A	N/A
Tubular Dilation	0.77	0.92	0.97
Tubular Degeneration/Regeneration	0.95	0.85	0.91
Interstitial Inflammation/Fibrosis	0.89	0.9	0.94
Crystals	N/A	0.81	0.88

changes (data available in the supplement). The scores were transformed into numerical values (no changes – 0, minimal – 1, mild – 2, moderate – 3, marked – 4). For calculating several of the correlation coefficient values, some of the manual scores were summed to facilitate more appropriate comparison: the degeneration score with the regeneration score, as well as the inflammation score with the fibrosis score. Histopathological evaluation of the studies is available in the supplementary material.

CONCLUSIONS

In summary, our results showed that image analysis technology provides robust analysis of multiple endpoints

in commonly used rat models of renal failure. The quantified histopathological changes such as glomerular expansion, tubular dilation, degeneration, and interstitial inflammation correlated with decreased renal function. The consistent algorithm set allowed for an objective analysis and helped define key characteristics, such as showing a very pronounced glomerular expansion in the 5/6 nephrectomy model or much more severe tissue inflammation in the adenine model.

Automated image analysis allows for the development of a useful and practical set of quantitative tools, showing unrestrained flexibility and customization. It offers an efficient approach for the consistent detection of quantifiable changes, which could escape human perception, due to scale or distribution that is hard to discriminate by traditional observation. One of the advantages of the technology is reliability and consistency in classification by avoiding human operator error, bias or fatigue. Moreover, whole slide image analysis is resistant to possible feature regional fluctuations, allowing for a marked increase in the number of elements analyzed, thus providing a more holistic assessment of tissue sections. Finally, automated analysis can be performed in a batch mode, without user supervision (e.g. overnight), saving time and human resources.

Another advantage of computer-aided image analysis is the opportunity it allows for greater synthesis between pathologists and biomedical scientists utilizing advanced image assessment modalities. Pathologists provide key inputs on essential factors affecting interpretation such as low quality data, which can be affected at any stage of sample collection and processing, as well as supply historical knowledge regarding the findings from previous studies and their relationship to current investigations. An important caveat to remember is that extreme care must be taken while preparing slides for the analysis, and it is essential to rely on experienced personnel for tissue preparation and to employ automation whenever possible.

Pattern recognition technology is far from being foolproof and cannot be used unverified. Each analyzed slide needs to be checked for quality. This varies from task to task, some algorithms perform flawlessly on hundreds of samples, and some need to be adjusted for each section, especially where analysis is based on staining color intensity. It is often needed to develop two separate Genie classifiers for a healthy and an injured tissue, especially where the morphology is markedly changed due to treatment. This is justified, as long as the classifier is subject for the same subsequent analysis algorithm. Due to the machine-learning nature of pattern recognition (relying on training sets), no algorithm will run with 100% efficiency, no matter how well the classifiers were developed; there always will be some misclassified regions. Therefore, it is crucial to have ongoing supervision and interaction between imaging scientists and pathologists as well as proper experimental controls, sufficient number of samples and appropriate statistical analysis.

REFERENCES

1. Pantanowitz L, Valenstein PN, Evans AJ, Kaplan KJ, Pfeifer JD, Wilbur DC, *et al*. Review of the current state of whole slide imaging in pathology. J Pathol Inform 2011;2:36.
2. Feldman MD. Beyond morphology: whole slide imaging, computer-aided detection, and other techniques. Arch Pathol Lab Med 2008;132:758-63.
3. Friedberg RC, Pantanowitz L. Practice evolution: decentralized computer-assisted immunohistochemical image analysis. Arch Pathol Lab Med 2009;133:597-600.
4. Słodkowska J, Markiewicz T, Grala B, Kozłowski W, Papierz W, Pleskacz K, *et al*. Accuracy of a remote quantitative image analysis in the whole slide images. Diagn Pathol 2011;6 Suppl 1:S20.
5. Fallon MA, Wilbur DC, Prasad M. Ovarian frozen section diagnosis: use of whole-slide imaging shows excellent correlation between virtual slide and original interpretations in a large series of cases. Arch Pathol Lab Med 2010;134:1020-3.
6. Baumgarten M, Gehr T. Chronic kidney disease: detection and evaluation. Am Fam Physician. 2011;84:1138-48.
7. Toto RD. Treatment of hypertension in chronic kidney disease. Semin Nephrol 2005;25:435-9.
8. Lakovlev VV, Gabril M, Dubinski W, Scorilas A, Youssef YM, Faragalla H, *et al*. Microvascular density as an independent predictor of clinical outcome in renal cell carcinoma: an automated image analysis study. Lab Invest 2012;92:46-56
9. Brazdziute E, Laurinavicius A. Digital pathology evaluation of complement C4d component deposition in the kidney allograft biopsies is a useful tool to improve reproducibility of the scoring. Diagn Pathol 2011;6 Suppl 1:S5.
10. Meas-Yedid V, Servais A, Noël LH, Panterne C, Landais P, Hervé N, *et al*. New computerized color image analysis for the quantification of interstitial fibrosis in renal transplantation. Transplantation 2011;92:890-9.
11. Servais A, Meas-Yedid V, Buchler M, Morelon E, Olivo-Marin JC, Lebranchu Y, *et al.* Quantification of interstitial fibrosis by image analysis on routine renal biopsy in patients receiving cyclosporine. Transplantation. 2007;84:1595-601.
12. Shimamura T, Morrison AB. A progressive glomerulosclerosis occurring in partial five-sixths nephrectomized rats. Am J Pathol 1975;79:95-106.
13. Cortes P, Zhao X, Riser BL, Narins RG. Regulation of glomerular volume in normal and partially nephrectomized rats. Am J Physiol 1996;270:F356-70.
14. Kööbi P, Vehmas TI, Jolma P, Kalliovalkama J, Fan M, Niemelä O, *et al*. High-calcium vs high-phosphate intake and small artery tone in advanced experimental renal insufficiency. Nephrol Dial Transplant 2006;21:2754-61.
15. Jiang Y, Wang M. Hyperphosphatemia-induced hyperparathyroidism in 5/6 nephrectomized rats: development of a new animal model. Chin Med J (Engl) 2008;121:2440-3.
16. Custódio MR, Koike MK, Neves KR, Dos Reis LM, Graciolli FG, Neves CL, *et al*. Parathyroid hormone and phosphorus overload in uremia: impact on cardiovascular system. Nephrol Dial Transplant 2012;27:1437-45.
17. Yokozawa T, Zheng PD, Oura H, Koizumi F. Animal model of adenine-induced chronic renal failure in rats. Nephron 1986;44:230-4.
18. Ikeda R, Imai Y, Maruyama W, Mizoguchi K. Systemic disorders of calcium dynamics in rats with adenine-induced renal failure: implication for chronic kidney disease-related complications. Nephrology (Carlton) 2010;15:54-62.
19. Sakairi T, Hiromura K, Yamashita S, Takeuchi S, Tomioka M, Ideura H, *et al*. Nestin expression in the kidney with an obstructed ureter. Kidney Int 2007;72:307-18.